The representative topography of worn hot rolling mill cylinders

Emilie Luc, Maxence Bigerelle, Raphaël Deltombe, Mirentxu Dubar

The representative topography of worn hot rolling mill cylinders

E. Luc [a], M. Bigerelle [b,*], R. Deltombe [c], M. Dubar [b]

[a] Aperam Stainless Services & Solutions, Service Recherche, 62330 Isbergues, France
[b] Laboratoire LAMIH/TEMPO, UMR CNRS 8201, Valenciennes, France
[c] LAMIH, UMR CNRS 8201, Valenciennes, France

A B S T R A C T

In this paper, a method is proposed to extract the most representative surface topography from *n* surfaces. A criterion is proposed that allows rejecting irrelevant topographical maps. Then, this methodology is applied on the hot rolling process, on replicas of industrial surfaces. These analyses have shown the major difference between ICDP and HSS roll behavior in terms of topography. Carbides oxidation observations correlates lab studies from bibliography. We confirm that this methodology is relevant to industrial investigations, especially on phenomena requiring non-destructive protocol.

Keywords:
Roughness
Hot rolling process
Wear
Rolling mill rolls

1. Introduction

To minimize topographical error measurements, several roughness measurements are often performed on surfaces. This multi measurement is even more practiced due to automatism of 3D roughness apparatus. However, the huge amount of data becomes more and more difficult to be investigated and visually explored. A possible alternative consists in analyzing roughness parameters that may not require the surface observation. However, to the author's opinion, the visualization of the surface before computing parameters is of major importance to avoid bad measurements. After roughness parameters computation, surface visualization is also needed to analyze the physical meaning of parameters obtained by statistical analyses. In this paper, a method is proposed to extract the most representative surface from *n* surfaces.

2. The hot rolling process

2.1. General description of hot rolling

Hot rolling is a conventional manufacturing process of steel industry that allows obtaining a flat or long semi-product from a slab or a billet. After melting shop, the goal of this process step is to transform the slab into a thin sheet (2–4 mm) in successive reduction rate occurring at high temperatures, between 1300 °C and 500 °C. After hot rolling, several steps are required to pickle the metal and to reach accurate mechanical characteristics. Hot rolling process (Fig. 1) consists in reheating a slab during 3 h up to temperatures around 1250 °C. At the exit of a walking beam furnace, the slab is reduced in thickness from 200 mm to 40 mm in five to seven successive passes in a roughing mill. After this step, a secondary step of rolling induces a reduction of the product called transfer bar into a coil of 3 mm thick. This step is realized on the finishing mill. The strip is then quenched and coiled. The time required to roll one slab is around 3 min and the temperature of the transfer bar (before finishing mill) is around 1100 °C and, at the exit of the finishing mill, it is only 950 °C. Our study focuses on the finishing mill which is the second reduction step on hot strip mill line.

2.2. Description of the finishing mill

The finishing mill is a quarto-tandem mill that means that each stand is composed of two working rolls that are in direct contact with the product and two backup rolls that are used to support severe stress by reducing deflection. The finishing mill is a seven stands tandem mill: it means that the strip is trapped in the seven stands at the same time. The goal is to reduce the thickness of an entering product up to 90% in a few seconds, at an increasing speed of 0.1 m/s to 7 m/s. The transfer bar (intermediary state between slab and coil) will be introduced in seven successive stands that will reduce the thickness from 40 mm to 3 mm. During the rolling, the only controlled instructions of the finishing mill are the rolling temperature and the strip thickness after stand 7. The production schedule between stand 1 and 7 is fully automated and is modified by regulation system that can modify the reduction ratio and the speed of rolls during rolling in order to match the

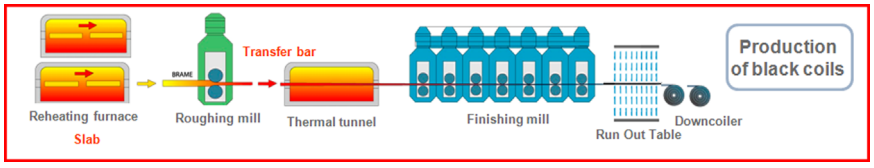

Fig. 1. Hot rolling of stainless steel strips with the seven stands finishing mill.

Table 1
Chemical composition of cylinders.

Cylinder Grade	C (%)	Ni (%)	Si (%)	Mn (%)	Cr (%)	V (%)	Mo (%)
HSS	2.0	1.5	0.7	1.0	4.4	5.2	5.4
ICDP	3.0	3.7	0.8	0.8	1.5	0.1	0.3

two conditions on strip thickness and temperature after stand 7. That is the reason why there is no conventional rolling pass schedule on tandem finishing mills.

2.3. Working rolls

There are two types of working rolls used in the finishing mill:

- HSS (high strength steel) grade located in *F*1, *F*2, *F*3 and *F*4.
- ICDP (indefinite chilled double pour) grade which is a cast iron roll located in *F*5, *F*6 and *F*7.

Our study will be focused on stand *F*4 and *F*5, where type of rolls is, respectively, HSS (high strength steels) and ICDP. Chemical composition of rolls is given in Table 1.

2.3.1. HSS rolls microstructure

Working rolls are composed of a hard matrix (martensitic structure) and Cr, Mo and V carbides are used to provide them a high wear resistance.

HSS rolls are mainly characterized by the presence of fine hard carbides, allowing on one hand to achieve higher shell hardness and on the other hand, to have higher resistance to wear and oxidation [1] (Fig. 2).

Carbides results from the addition of elements such as vanadium, molybdenum, tungsten and chromium that have a high affinity with carbon. M_7C_3 carbides and the molybdenum–vanadium type M_6C are mainly formed along grain boundaries while vanadium carbides of MC type are distributed within the grains [2,3]. M_2C carbides (due to the addition of W and Mo) may exist but are often mixed with the M_7C_3 and their fraction is so low that they are most often confused with them. In the matrix, we can also find some very fine spheroidal carbides of $M_{23}C_6$ type.

SEM examination of HSS roll highlighted (Fig. 2) that carbides are of different types:

- in white, the molybdenum–vanadium carbides, which are located on the grain boundaries are representing 9% of the surface of the roll;
- in black, are represented the MC type Vanadium carbides, essentially located in the grains, are representing only 2% of the surface.

Chromium carbides are surrounding the MC type vanadium carbides in the grains.

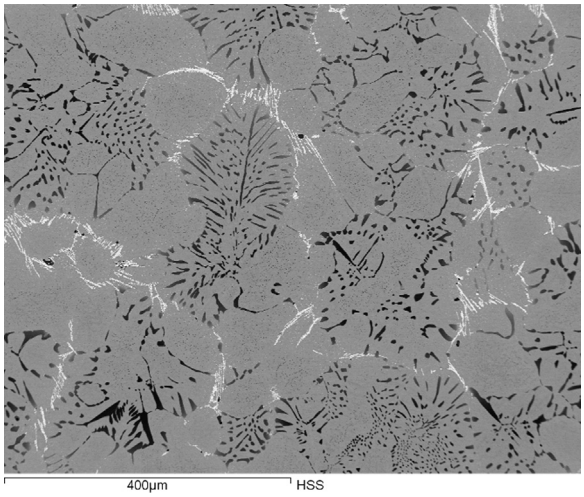

Fig. 2. SEM examination of HSS microstructure with presence of two carbides (white and black forms).

2.3.2. ICDP roll microstructure

ICDP rolls have a double precipitation: they have both graphite and coarse carbides M_3C type—Fe_3C (cementite-white) (hence the name "indefinite quenching"). The proportion of graphite is comprised between 1% and 3%, while the fraction of carbide is significantly greater, between 35% and 45% (Fig. 3). ICDP rolls have a mixed martensite/bainite matrix and their particularity is that the chemical composition of the shell varies with the radius. The higher the radius, the lower the free C (graphite) content; so, the lower the carbides amount. This leads to a decrease in shell hardness with roll wear. The roll hardness decrease leads to a rapid wear and therefore, to a regular roll change during production schedule. The main consequence is a reduction in productivity and additional cost of consumables. There is no drop in hardness with decreasing radius of the HSS. Due to high interaction between the roll and the steel product, we are interested in characterizing the roughness of the roll in order to understand well the evolution of roughness on the steel strip. That is why some investigations on roughness measurement on industrial working rolls were done.

3. The 3D surface measurements

3.1. Replicas on hot mill roll

In order to better characterize the surface of working rolls, and because of their large dimensions (from 680 mm to 760 mm in diameter and 2.5 m long), some replicas onto the surface of the work roll were performed.

On ferritic stainless steel production schedule, only three different strip widths are processed on the hot rolling mill of APERAM. Indeed, samples at four different chosen areas were taken: the first one was taken in the middle of roll length, corresponding to the center of the strip (of each width size), which correspond to the position C. A second sample was taken at

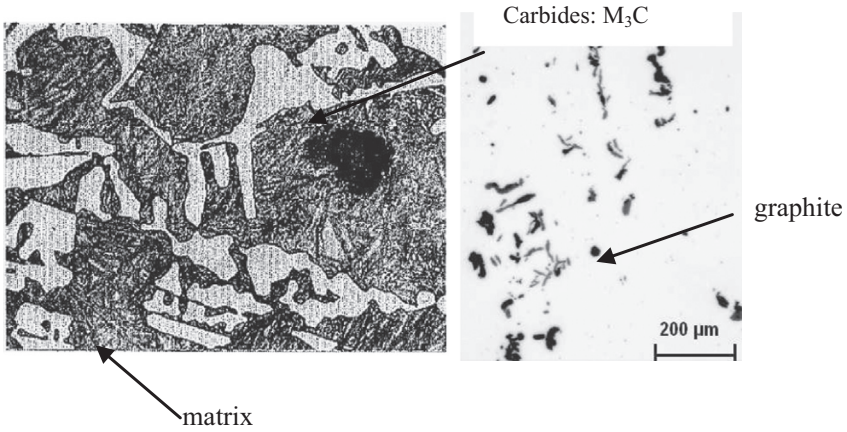

Fig. 3. SEM Microstructure of ICDP cylinders.

60 cm form the previous position in direction to the motor side, corresponding to strip width of 1300 mm. A third sample was taken at 70 cm from the middle of the roll (strip width of 1500 mm). A last sample was taken at 1 m from the middle. No ferritic strip of 2 m wide are produced, as a result, the surface taken as last sample correspond to a non-worn part of the roll by strip rolling. Superior and inferior rolls were analyzed (Fig. 4). Replicas were made using the Repliset *T*3 resin (proposed by Struers®) after cleaning of roll surface with cleaning agent and ethanol.

Samples were identified by the roll number, the position along roll length (middle, 1300 mm, 1500 mm, 2 m), strip length rolled with it. Because HSS rolls have very good surface aspect (by visual inspection) after the processing of one conventional ferritic schedule, it was decided to increase the number of coils processed with the same working roll pair. As a result, we are able to analyze the evolution of roughness after 50 km processed and after 500 km by the same roll pair.

Fig. 4. Position of samples on working cylinder pair.

3.2. Roughness measurements

The white light interferometer (NewView 7300, Zygo) is used for characterizing and quantifying surface roughness. Optical resolutions of $\times 20$ Mirau objective used are 0.71 µm for x and y axes based on Sparrow criterion which takes into account the lens numerical aperture and 0.01 µm for z axis. Indeed, spatial sampling based on camera pixel size (0.55 µm) is lower than the optical resolution. The inspected surface area is 1200 µm by 900 µm obtained by stitching 16 of each single measurement with 20% overlap. Fig. 5 represents the 3D topography map corresponding to the superior roll of stand *F*3 after 500 km rolling. Five surfaces are measured on each sample. Five surfaces are measured on each surface.

3.3. The multi-scale decomposition

The multiscale decomposition of the surface is particularly appropriate to analyze machining process [4]. The Gaussian filter has been recommended by ISO 11562-1996 [5] and ASME B46.1-1995 [6] standards for determining the mean line in surface metrology. This filter was adapted in order to filter the 3D surfaces with a given cut-off value [7]. In this study, only the high pass filter will be presented (for the sake of simplicity, we omitted the results of pass band filter because best parameters were not relevant in this study). Our system is used to filter all surfaces with different cut-off in order to obtain a multi-scale decomposition. The 30 consecutive steps are used in this decomposition, with a cut-off varying from 2 µm to 360 µm. Fig. 6 represents three high pass filters and three low pass one for surface decomposition. When the cut-off decreases, microscopic details appear on filtered surfaces.

Then, 3D Roughness parameters are computed. 3D roughness parameters are defined by the following standards: ISO 25178 [8] define 30 parameters, EUR 15178N [9] also define 30 parameters but some of them are identical to those of ISO 25178 [8]. Only 16 parameters are the latest ones. However, S_z (maximum height of surface roughness) and S_{td} (texture direction) are calculated differently in both standards. Further, seven 3D roughness parameters related to surface flatness are defined by ISO 12781 [10], and ASME B46.1 [6] defines seven similar parameters as ISO 25178 standard [8] (with different predefined filters) and one new parameter S_{Wt} (area waviness height). To sum up, 56 different 3D roughness parameters will be considered in this study. The 3D roughness parameters (see Table 2) can be classified into the following groups: amplitude parameters, spatial parameters, hybrid parameters, functional parameters, feature parameters, other 3D parameters.

4. Concept of selection of the representative topography

In a large number of surface studies, several roughness measurements must be proceeded to increase the statistical parameters robustness. The variability of roughness parameters can be split into two classes of variation. The first one can be linked to

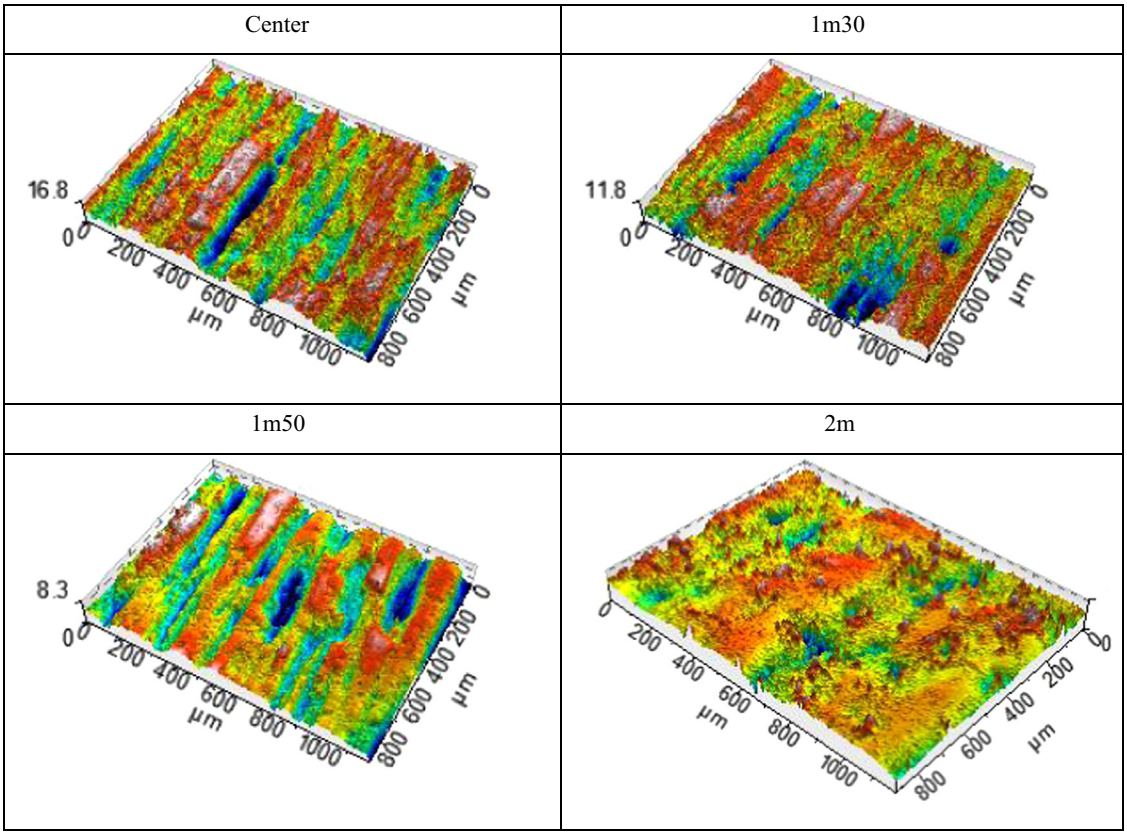

Fig. 5. Evolution of the topography along the axis cylinder in meter corresponding to the upper third cylinder after 500 km of wear.

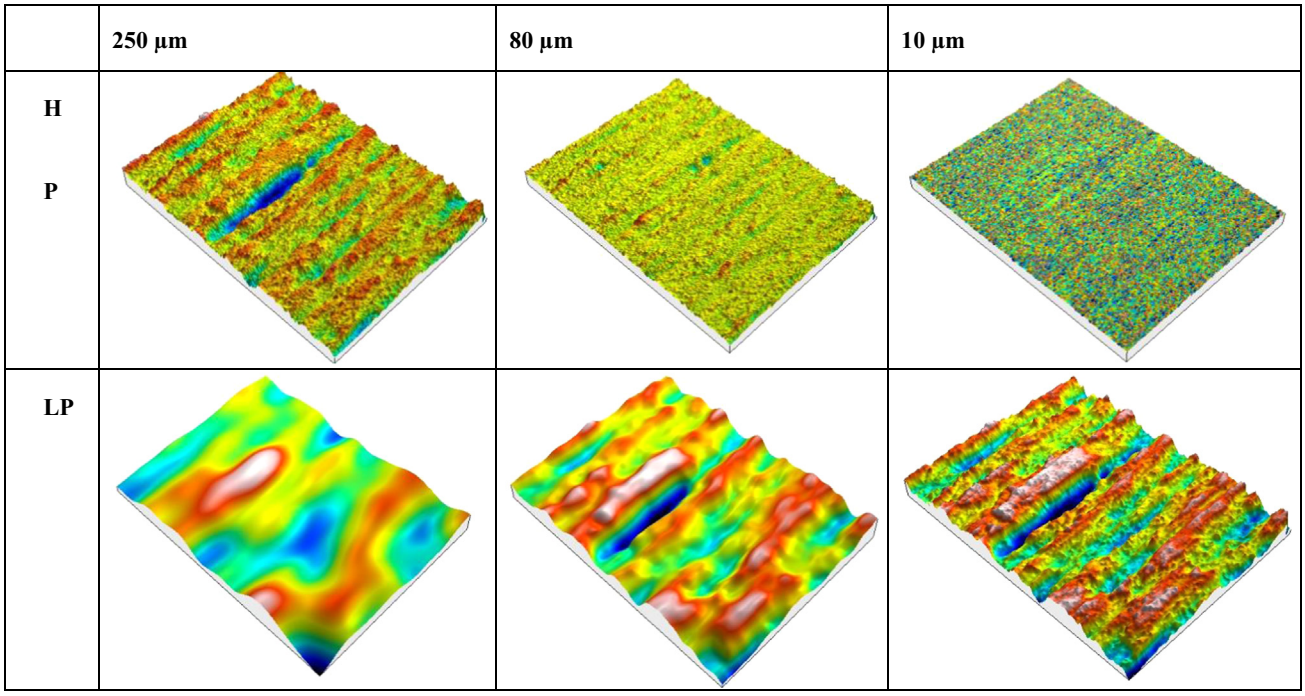

Fig. 6. Examples of multiscale decomposition using Gaussian high pass (HP) and low pass (LP) filtering at cut off 250 µm, 80 µm and 10 µm corresponding to the upper third cylinder after 500 km of wear measured at the center of the cylinder (see Fig. 1).

roughness apparatus. The topography map can differ even if the measurements are made on the same surface in the same area. This provides very smooth systematic instrument errors with essentially no contribution in the mid to high spatial frequencies of surface waviness and roughness. The random noise *N* generally includes shot noise and electronic noise in the fringe camera, artifacts from the acquisition process, as well as refractive index variations in the interferometer due to air turbulence. Furthermore, averaging of measurements reduces the random noise as long as longer term system drifts or instabilities don't limit the

noise reduction. In other part, errors occur from the surface itself. In our case, as in a number of engineering surfaces, surfaces are random. This means that amplitude topography map contains a random part. If the surface was infinite, then roughness parameters would be perfectly known. As it is not the case, roughness parameters computed from experimental maps can be seen as estimators of the surface topography and possesses a variance due to sampling. As a consequence, several measurements of surfaces have to be made in order to estimate the number of surfaces that enables to reach a good statistical convergence of the roughness parameters. As roughness apparatus allows automatic measurements of different areas of the surface, one reaches an amount of topographical maps so large that they cannot be all visualized. Three ways of dealing with this issue can be chosen:

- Due to the large numbers of maps, only roughness parameters are analyzed versus physical parameter of the process (process elaboration, integrity properties, and functionality properties).
- All the surfaces are visualized and perhaps it can be possible to clearly deduce some properties. However, the number of surfaces can be very large and such visualization required software that does not exist yet.
- For only one configuration, only one experimental surface that represents the entire measured surface is proposed.

The third case will be treated in this article. The basic aspect is to give a methodology that will only visualize a surface that is the "closest" (in a topographical sense) to all the measured surfaces processed in a same condition to compare all different experimental situations. This surface will be called the "relevant surface". Conversely, a surface that is "too different" can be seen as irrelevant surfaces due to error having different causes (scratch, pit, error measurement, …) will be an irrelevant surface.

The meaning of the expression "relevant surface" must be split into two groups:

The metrological relevance: in this case, the surface will be retained to be representative of the group of measured topographical maps of one surface.

The physical relevance: in this case, the surface will be retained to be representative of the influence of a given physical parameter that influences the surface morphology.

Table 2
3D roughness parameters calculated and analyzed in this study.

3D roughness parameters			
Symbol	Units	Name of parameter	Standard
Amplitude parameters			
S_q	µm	Root mean square height	ISO 25178
S_{sk}	–	Skewness	ISO 25178
S_{ku}	–	Kurtosis	ISO 25178
S_p	µm	Maximum peak height	ISO 25178
S_v	µm	Maximum pit height	ISO 25178
S_z	µm	Maximum height	ISO 25178
S_a	µm	Arithmetic mean height Total height	ISO 25178
S_t	µm		EUR 15178N
Spatial parameters (ISO 25178)			
S_{al}	mm	Auto-correlation length	ISO 25178
S_{tr}	–	Texture-aspect ratio	ISO 25178
S_{td}	°	Texture direction	ISO 25178
S_{al}	mm	Fastest decay autocorrelation length	ISO 25178
Hybrid parameters (ISO 25178)			
S_{dq}	–	Root mean square gradient	ISO 25178
S_{dr}	%	Developed interfacial area ratio	ISO 25178
S_{ds}	$1/mm^2$	Density of summits	EUR 15178N
S_{sc}	1/mm	Arithmetic mean summit curvature	EUR 15178N
S_{fd}	–	Fractal dimension of the surface	EUR 15178N
Functional parameters			
S_k	µm	Core roughness depth	EUR 15178N
S_pk	µm	Reduced summit height	EUR 15178N
S_{vk}	µm	Reduced valley depth	EUR 15178N
S_{r1}	%	Upper bearing area	EUR 15178N
S_{r2}	%	Lower bearing area	EUR 15178N
S_{pq}	–	Plateau root mean square roughness	EUR 15178N
S_{vq}	–	Valley root mean square roughness	EUR 15178N
S_{mq}	–	Material ratio at plateau-to-valley transition	EUR 15178N
S_{mr}	%	Areal material ratio	ISO 25178
S_{mc}	µm	Inverse areal material ratio	ISO 25178
S_{xp}	µm	Extreme peak height	ISO 25178
S_{dc}	µm	Areal height difference	ISO 25178
Volume functional parameters			
V_m	mm^3/mm^2	Material volume	ISO 25178
V_v	mm^3/mm^2	Void volume	ISO 25178
V_{mp}	mm^3/mm^2	Peak material volume	ISO 25178
V_{mc}	mm^3/mm^2	Core material volume	ISO 25178
V_{vc}	mm^3/mm^2	Core void volume	ISO 25178
V_{vv}	mm^3/mm^2	Pit void volume	ISO 25178
Functional indices			
S_{bi}	–	Surface bearing index	EUR 15178N
S_{ci}	–	Core fluid retention index	EUR 15178N
S_{vi}	–	Valley fluid retention index	EUR 15178N
Feature parameters			
S_{pd}	$1/mm^2$	Density of peaks	ISO 25178
S_{pc}	1/mm	Arithmetic mean peak curvature	ISO 25178
S_{10z}	µm	Ten point height	ISO 25178
S_{5p}	µm	Five point peak height	ISO 25178
S_{5v}	µm	Five point pit height	ISO 25178
S_{da}	mm^2	Mean dale area	ISO 25178
S_{ha}	mm^2	Mean hill area	ISO 25178
S_{dv}	mm^3	Mean dale volume	ISO 25178
S_{hv}	mm^3	Mean hill volume	ISO 25178
Other 3D parameters (from Mountain™ software)			
S_{mean}	µm	Mean height in absolute	No standard
S_{dar}	mm^2	Developed area	No standard
S_{par}	mm^2	Projected area	No standard
–	$µm^3$	Mean volume of islands	No standard
–	µm	Mean height of islands	No standard
–	$µm^2$	Mean surface of islands	No standard

5. Selection of the representative metrological topography

5.1. Principle of the method

The aim of this work is to select the topography that is the most representative of the whole surface. This philosophy allows us to select only one topography to be visualized that will be more comfortable to analyze process in other study. For each sample, N measures are performed. Then, different filtering cut-offs are

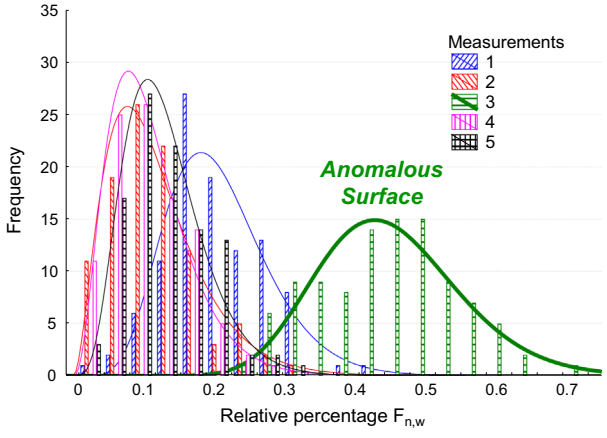

Fig. 7. Analyze of the F_n PDF for the anomalous surface corresponding to the five surfaces taken at of a worn cylinder Stand *F*2, 53 km, inferior, center.

performed to reconstruct roughness and waviness of the surface leading to computation of $p_{i,\varepsilon,c,n}$ roughness parameters related to the nth surfaces ($i \in \{1 \ldots I\}$) computed at the filter c with a cut off ε. Then, the mean of each roughness parameter computed from the N surfaces is evaluated leading to $\overline{p}_{i,\varepsilon,c}$ and standard deviations $\sigma_{i,\varepsilon,c}$. The indicator $q_{i,\varepsilon,c,n}$ is then proposed for the nth surfaces:

$$q_{i,\varepsilon,c,n} = \left(\frac{p_{i,\varepsilon,c,n} - \overline{p}_{i,\varepsilon,c}}{\sigma_{i,\varepsilon,c}} \right)^2 \tag{1}$$

Then, the optimal surface seen by the $p_{i,\varepsilon,c}$ for the n surfaces is given by:

$$n_{\text{opt}}(i,\varepsilon,c) = \frac{n}{\min\limits_{n \in N} q_{i,\varepsilon,c,n}} \tag{2}$$

The different "best" surfaces $n_{\text{opt}}(i,\varepsilon,c)$ are counted to plot the frequency histogram that represents the number of multi-scale parameters seen as better for the n surfaces and is noticed $F_{n,\text{opt}}$.

Finally, the most representative n_{opt} surface is given by:

$$n_{\text{opt}} = \frac{n}{\max_{n \in N} F_{n,\text{opt}}} \tag{3}$$

This relation claimed that the most representative surface is close to the mean of all surfaces characterized by all roughness parameters computed at all scales.

At the contrary, the less representative surface will be given by:

$$n_w = \frac{n}{\max_{n \in N} F_{n,w}} \tag{4}$$

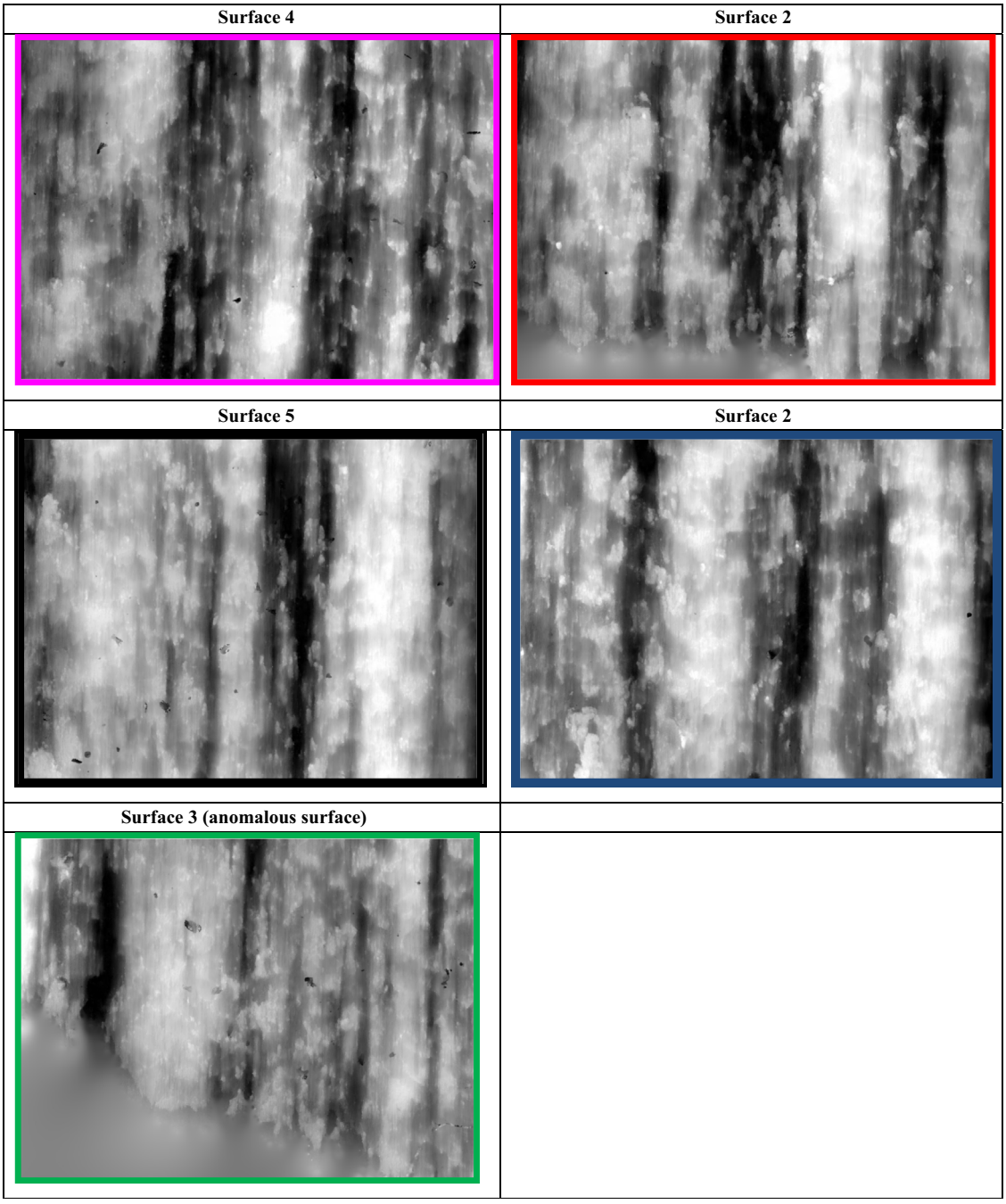

Fig. 8. Similar topographical images on the center of a worn cylinder Stand *F*2, 53 km, inferior, centre.

with

$$n_w(i,\varepsilon,c)=\frac{n}{\max_{n\in N} q_{i,\varepsilon,c,n}} \tag{5}$$

Surface n_w can be considered as irrelevant if statistically $F_{n_w,w} > F_{n,w}$, $n\in\{1\ldots N\}$, $n\neq n_w$. This method allows us to find surfaces that are badly recorded or present some defects and must be excluded from analyses. We will define these surfaces as irrelevant surfaces. However, to statistically prove that $F_{n_w,w} > F_{n,w}$, we have to design an original protocol to construct the probability density function of each $F_{n,\mathrm{opt}}$ and $F_{n,w}$. So, we decide to use the bootstrap philosophy to setup an estimator of the probability density function.

5.2. Construction of the relevance function probability density function,: the bootstrap protocol

In order to include the robustness of roughness parameters relevance, bootstrap is used. That allows estimating the error in the computation of statistical modeling coefficients. For these reasons, we have to introduce a recent technique called the bootstrap, which is a resampling technique [11,12]. The basic idea of the bootstrap is to create a new dataset by randomly sampling with replacement from the original data set and then performing the same statistical analysis as carried out on the original data set.

5.3. Irrelevant metrological surfaces

Let know search from all measurements (96 series of measures) if one gets a surface that can be seen as irrelevant. For that, we process 100 bootstraps. These steps allow us to suppress irrelevant measures and selected the most representative one. The next step in the analysis is to compute the mean Probability Density Function (PDF) of the F_n for all parts of the 14 rolls. Then, visually, irrelevant surface can be easily found and suppressed from analyze. For example, a suspicious surface is found and represents the Stand *F*2, 53 km, inferior roll, and center. Fig. 7 represents the value of these F_n PDF for this part of measurement (histograms). F_3 is seen higher than others F_n and can be seen as not representative or irrelevant. It can be observed that the irrelevance is very high because no overlap appears and surface 3 can be seen as different from others, so must be excluded. Looking on images (Fig. 8), it can be observed that this image presents an abnormal smoothing in the bottom left part: it is due to a bad replication of the surface by the elastomer.

5.4. The representative metrological surface

Let know search from all measurements (96 series of measures) if one to select the most relevant surface for all replicas. After removal of irrelevant surfaces (see Section 5.3), we process again to new analyses with 100 bootstraps. The next step in the analysis is to calculate the mean Probability Density Function (PDF) of the F_n for all parts of the 14 rolls. Let now analyze an example: for Stand *F*2, 53 km, inferior roll, 2 m (Fig. 9). Fig. 10 represents the value of these F_n PDF for this part of measurement (histograms). F_3 is seen lower than others F_n and can be seen as the most representative surface.

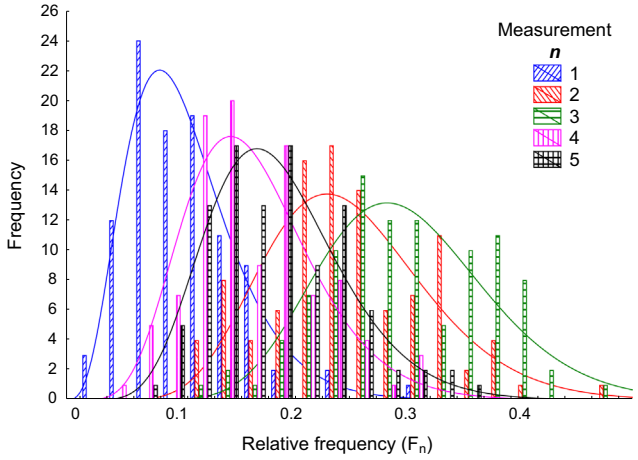

Fig. 9. Analyze of the F_n PDF for the anomalous surface corresponding to the five surfaces taken at of a worn cylinder Stand *F*2, 53 km, inferior, 2 m.

6. Selection of the representative physical topography

6.1. Principle of the method

It is expected that some of the identified parameters are not at all useful while others are relevant. Hence, it would be appropriate to consider some weighting, or at least to limit the consideration of parameters only to those that are relevant. Otherwise, the optimization cannot give relevant results as an unjustified importance was given to rather useless parameters. As an example, 5% of the samples may contain roughness defects. The latter are critical to understanding roughness evolution, but the optimization method would treat these as not representative.

In this part we will first define the weighted method and then analyze the representative surface that depicts the effect of wear, position on the rolling process and the effect of the lateral position of the roll. Interaction between these three parameters will not be treated.

6.2. The weight function

To find the weight function, the analysis of variance (ANOVA) will be used. It is an implementation of the general linear model, which is a powerful technique to test the relevance of our approach. In our case, the ANOVA model can be stated as follows:

$$p_i(\varepsilon,c,k_1,k_2,\ldots,k_p,n) = \alpha_0+\sum_{j=1}^{p}\alpha_{j,k_j}(i,\varepsilon,c)+\sum_{j=1}^{p}\sum_{l=j+1}^{p}\beta_{j,k_j,l,k_l}(i,\varepsilon,c)+\xi_{k_1,k_2,\ldots,k_p,n}(i,\varepsilon,c) \tag{6}$$

where $p_i(\varepsilon,c,k_1,k_2,\cdots,k_p,n)$ is the value of the roughness parameter p_i of the *n*th surface when the p process parameters are taken at levels $k_1,k_2,\ldots,k_p$, for filtered surface with a c-pass filter of cut off ε; $\alpha_{j,k_j}(\varepsilon,c,L)$ is the influence of the roughness value of the *j*th process parameter at level k_j; $\beta_{j,k_j,l,k_l}(i,\varepsilon,c)$ is the influence of the interaction value between both process parameters k_j and k_l; $\xi_{k_1,k_2,\ldots,k_p,n}(i,\varepsilon,c)$ is a Gaussian noise with null mean value and standard deviation σ.

The program will first compute the within-cell variance/covariance matrix of process variables (and covariates). The design matrix of main effects and interactions is first ortho-normalized, and then used to compute the sums of square hypotheses (from the cell means) and sums of square errors (from the within-cell variance/covariance matrix). The output of the analysis includes statistical information about the levels of the variable process under analysis i.e. the degrees of freedom, sum of squares and the

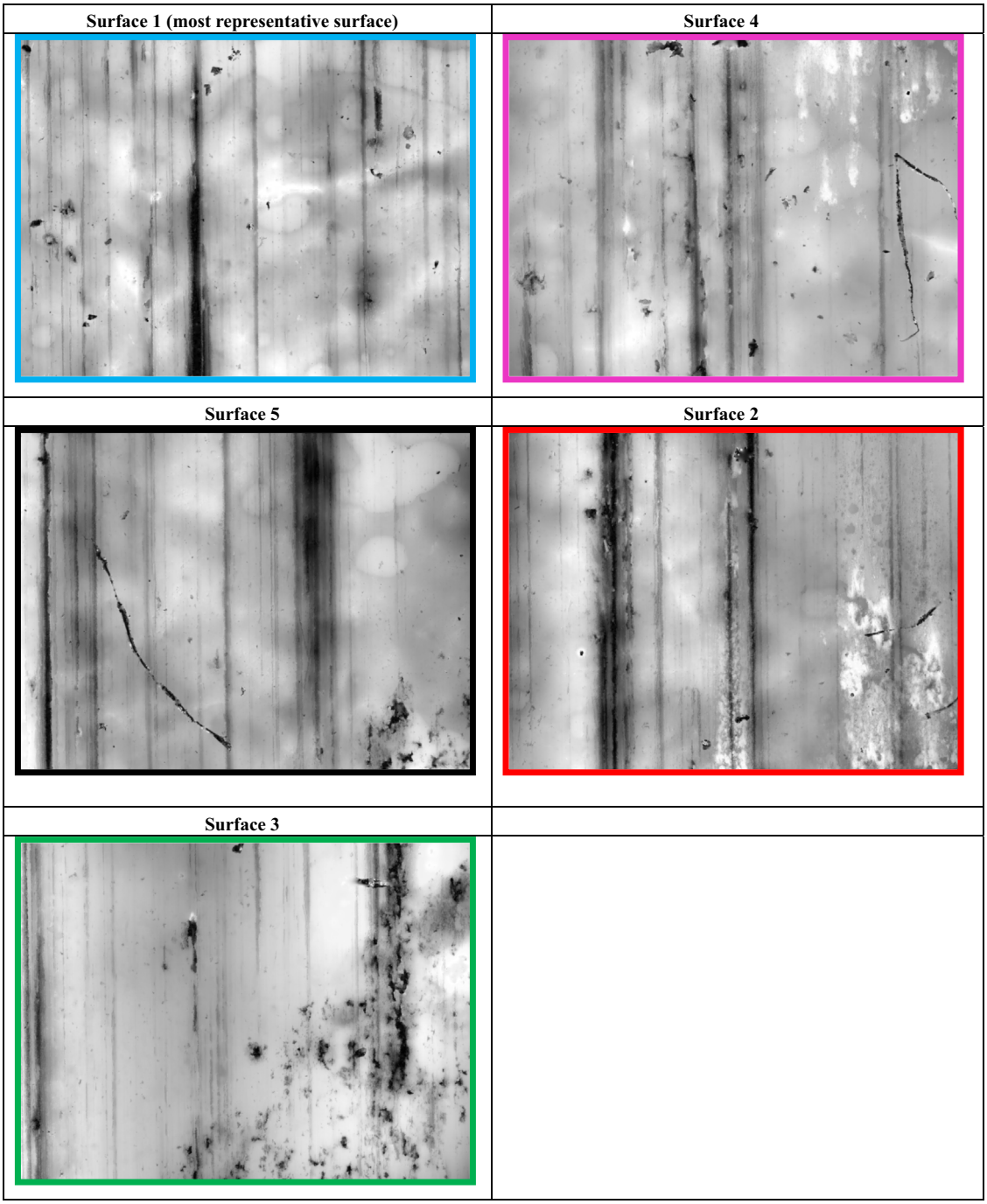

Fig. 10. Similar topographical images on the center of a worn cylinder Stand *F2*, 53 km, inferior, 2m.

mean square for the model and for random error. "Root MSE" is the square root of the mean square for error. Our weight function will be the Fisher variation $\Phi[p_i(\varepsilon, c, k_j)]$ value, which is the ratio produced by dividing the mean square for the model at configuration j. If the model does not really affect the expected value of the response, then the two mean square values should be about the same ($\Phi[p_i(\varepsilon, c, k_j)] \cong 1$); on the contrary a model mean square much larger than the error mean square ($\Phi[p_i(\varepsilon, c, k_j)] \gg 1$), indicates that the model does in fact affect the response. To reject the fact that a process parameter does not modify the surface roughness parameters, the relation $\Phi[p_i(\varepsilon, c, k_j)] > \Phi_0(\theta)$ must hold, where $\Phi_0(\theta)$ is a Fisher variable at a confidence interval θ. The higher θ, the lower the probability to affirm wrongly that a process parameter influences a roughness parameter.

From Eq. (1), the new weighted parameters by the k_j process parameter is proposed:

$$\hat{q}_{i,\varepsilon,c,k_j} = \Phi[p_i(\varepsilon, c, k_j)]\left(\frac{p_{i,\varepsilon,c,n} - \overline{p}_{i,\varepsilon,c}}{\sigma_{i,\varepsilon,c}}\right)^2 \tag{7}$$

All the calculations described in Section 5.1 leads to construct the most representative surface $\hat{n}_{\text{opt}}(k_j)$ for the process k_j.

6.3. Expression analyses of the weight function

The weight function can be plotted for the three processes (Fig. 11). As it can be observed, some roughness parameters are relevant while others are not relevant. The highest value of the

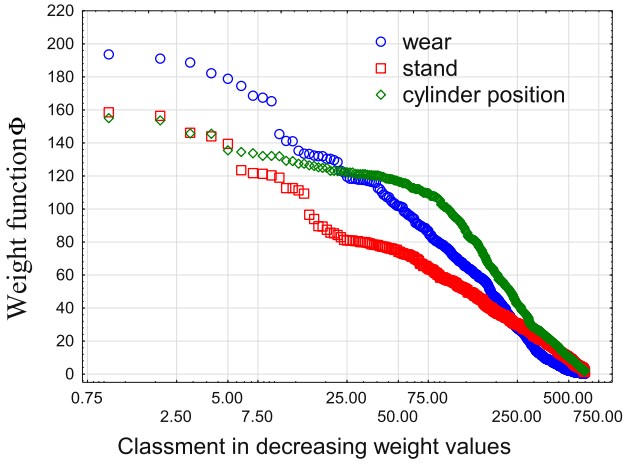

Fig. 11. Plot of the weight function $\Phi[p_i(\varepsilon, c, k_j)]$ for the three process conditions (wear, stands, and cylinder position).

Table 3
Value of the weight function corresponding to the highest value for the three processes. The roughness parameters with their appropriate scales are sum up in the table.

Filter	Cut off	Roughness	Process	$\Phi[p_i(\varepsilon, c, k_j)]$			
c	ε	$p_i(\varepsilon, c, k_j)$	k_j	Mean	95th percentile	Median	5th percentile
LP	75 μm	Furrows density	Stand	184	211	183	161
LP	9 μm	Number of motifs	Wear	199	288	194	122
HP	140 μm	V_{mc}	Position	159	200	158	125

weighted function is reported on Table 3. The density of furrows with low pass filter using a cut off of 75 μm well distinguishes the effect of stand (Fig. 12). The wear is well characterized by the number of motifs with a low pass filter using a cut off of 9 μm. Finally, the effect of the position along the roll is characterized by the V_{mc} with a high pass filter using a cut off of 140 μm.

6.4. *Visualization of the most representative maps including processes*

6.4.1. *Wear effect*

Fig. 13 shows the relevant topography at the whole scale and the relevant scale. As it can be observed, wear effects change roughness from isotropic structure to anisotropic structure with large bands.

6.4.2. *The stand effect*

From Fig. 14, it becomes evident that the effect of stand is principally due to change between stand *F*4 and *F*5. For the four first stands, roughness is given by large bands having a high amplitude. At the contrary, for stand *F*5 to *F*7, roughness amplitude is less important and roughness appears to be isotropic.

6.4.3. *The position in the roll effect*

From Fig. 15, the structure in the center of the roll is more damaged than those at its tail. Structure amplitude is more isotropic and fine with lower roughness amplitude on the tail of the roll (> 1m30) and less isotropic in the middle of the roll with band structure and rough amplitude (< 1m30).

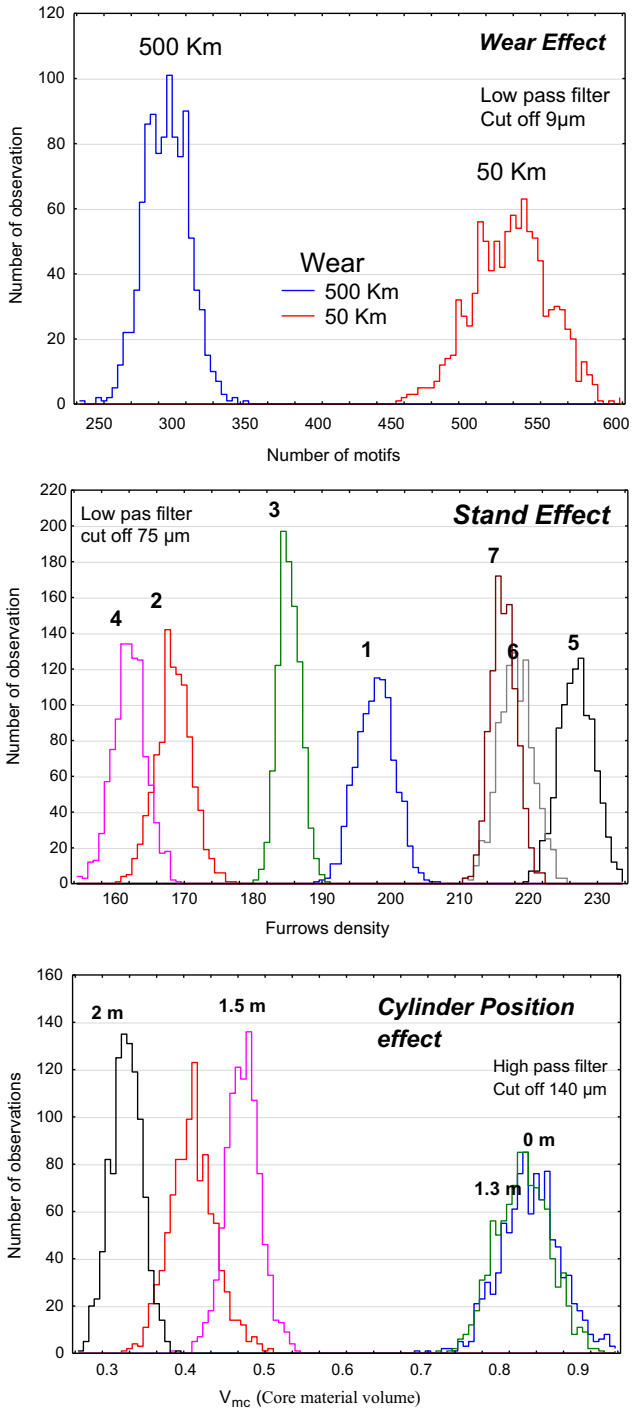

Fig. 12. Evolution of the roughness parameters corresponding to the maximal value of the weight function for the three processes wear, cylinder position and stands.

7. Discussion

The method is then applied to a complex system: the wear of rolls of a seven stands tandem hot rolling mill. At different zones of the roll, replicas are done during process on all rolls at different lateral positions. Our algorithm is then applied. Then the most representative images are used to analyze wear. Analyze of replicas gives detailed information of the roll wear. We will focus topography of roll surface on stand *F*4 and *F*5 because this was shown by our analyses to be different topographies (Fig. 14).

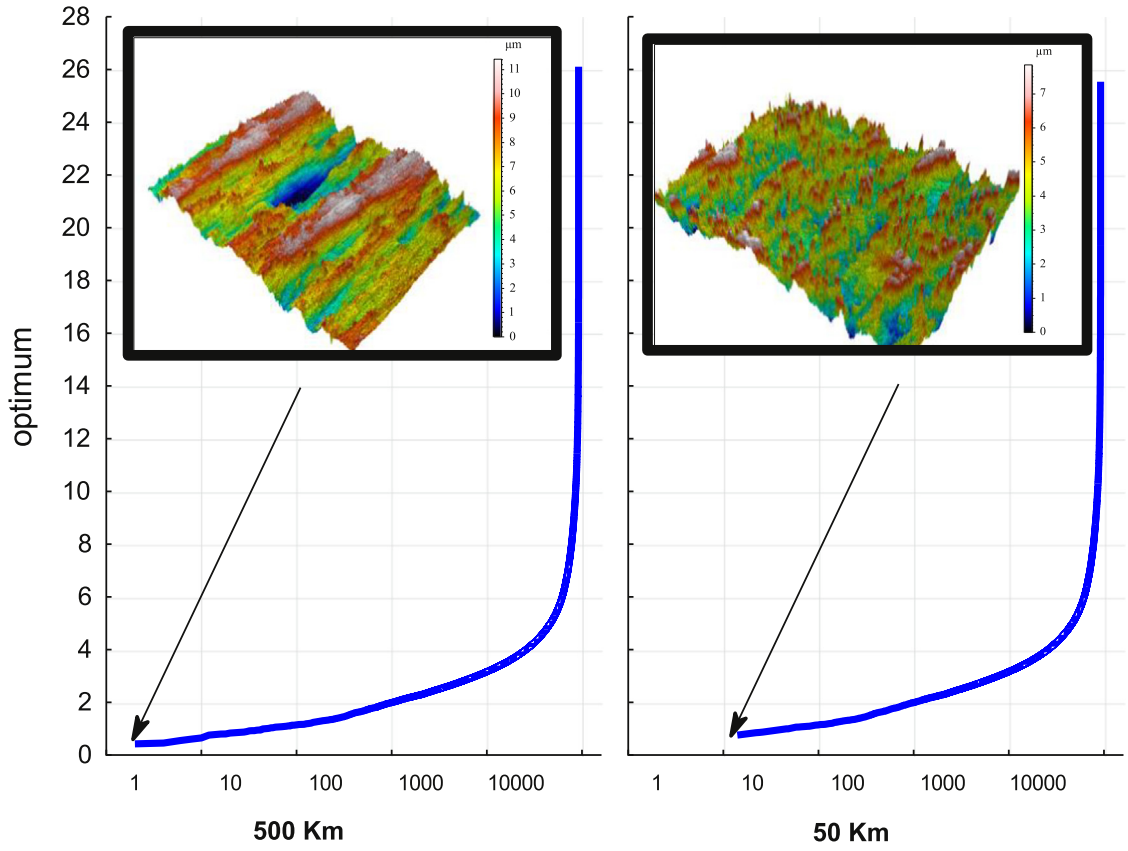

Fig. 13. Evolution of the representative topography for small wear (50 km of rolling) and high wear (500 km of rolling). The optimal function $\hat{q}_{i,e,c,k_j}$ is plotted for both stages of wear.

7.1. Stand F4

As already explained in Section 2.3, there is no ferritic production in 2 m wide. We can observe small dots (in red). These dots seems to make round shapes on the surface whose diameter is about 100 µm. Grain size on HSS roll can be observed on Fig. 2, and have a similar size, around 100–200 µm in diameter. We suspect that these dots are the carbides located in grain boundaries oxided by roll heating during rolling. This phenomenon was highlighted by several authors [13–15] that pointed out that all carbides start to oxidize before the matrix and within carbides, the MC type carbides containing Vanadium is the first to be oxidized, at 550 °C after 30 min in dry air. Moreover, thanks to the description of carbides oxidation made in [13], we think that dot areas of Fig. 15 (corresponding to unworn areas of the roll) correspond to a grain covered by vanadium carbides.

The replica corresponding to 1.5 m strip width is quite simple to analyze. The first production schedule rolled coils up to 1300 mm width and the second one rolled up to 1550 mm coil width. As a result, we can notice that on the superior and inferior roll, all replica corresponding to the short campaign (52 km) as similar to the replica corresponding to 2 m width, inferior roll, 52 km. So, the topography corresponds to the oxidation of carbides due to thermal conduction in the roll. On replicas corresponding to the long campaign (500 km), large stripes can be easily found on the surface. These large stripes are induced by edge rolling.

The replicas corresponding to 1.3 m coil width are more equivalent between the superior and inferior roll. We clearly observe a difference between the short (52 km) and the long campaign (500 km). On the short campaign, stripes seems to be larger but with a lower density, contrary to the long campaign where stripes seems to be thinner but the density of these stripes seems to be higher. It could be explained by the fact that on the short campaign, these stripes correspond to the rolling of coils edges of 1300 mm width, representing a side effect. On the long campaign, stripes due to edge rolling will be affected (partially erased?) by rolling of wider coils, so the large stripes will be eroded by the rolling of smoother surfaces. The replicas corresponding to the middle of roll length, so to the middle of the coil, are more homogeneous. Thin stripes are observed on replicas corresponding to the short campaign and more severe stripes (higher amplitude) are observed for the long campaign, translating a more severe wear.

7.2. Stand F5

Topography of the replica presented in Fig. 14 is different for the *F*5 stand than the *F*4 one. The major difference between the two stands is that the fifth stand is associated to ICDP rolls for rolling of ferritic stainless steels. Replicas concerning the 2 m position are characterized by small (red) dots randomly spread over the roll surface. There is no specific geometric shape associated to the position of these dots. The density of these dots seems is higher on the replicas corresponding to the long campaign (500 km). The height of these dots is around 7 µm to 16 µm, which is very high compared to the values found on *F*1–*F*4 stands.

We notice that the height of dots tends to decrease with length of coil rolled on worn areas (center, and 1.3 m width) and between the ground and worn areas: the higher the wear, the lower the height of the dots. Nevertheless, these results are opposed in terms of dots density. The maximal is reached on the replica corresponding to the center of the roll, the long campaign (500 km). Based on observations made by Ziehenberger et al. [16], these dots could be due to oxidation of carbides at roll

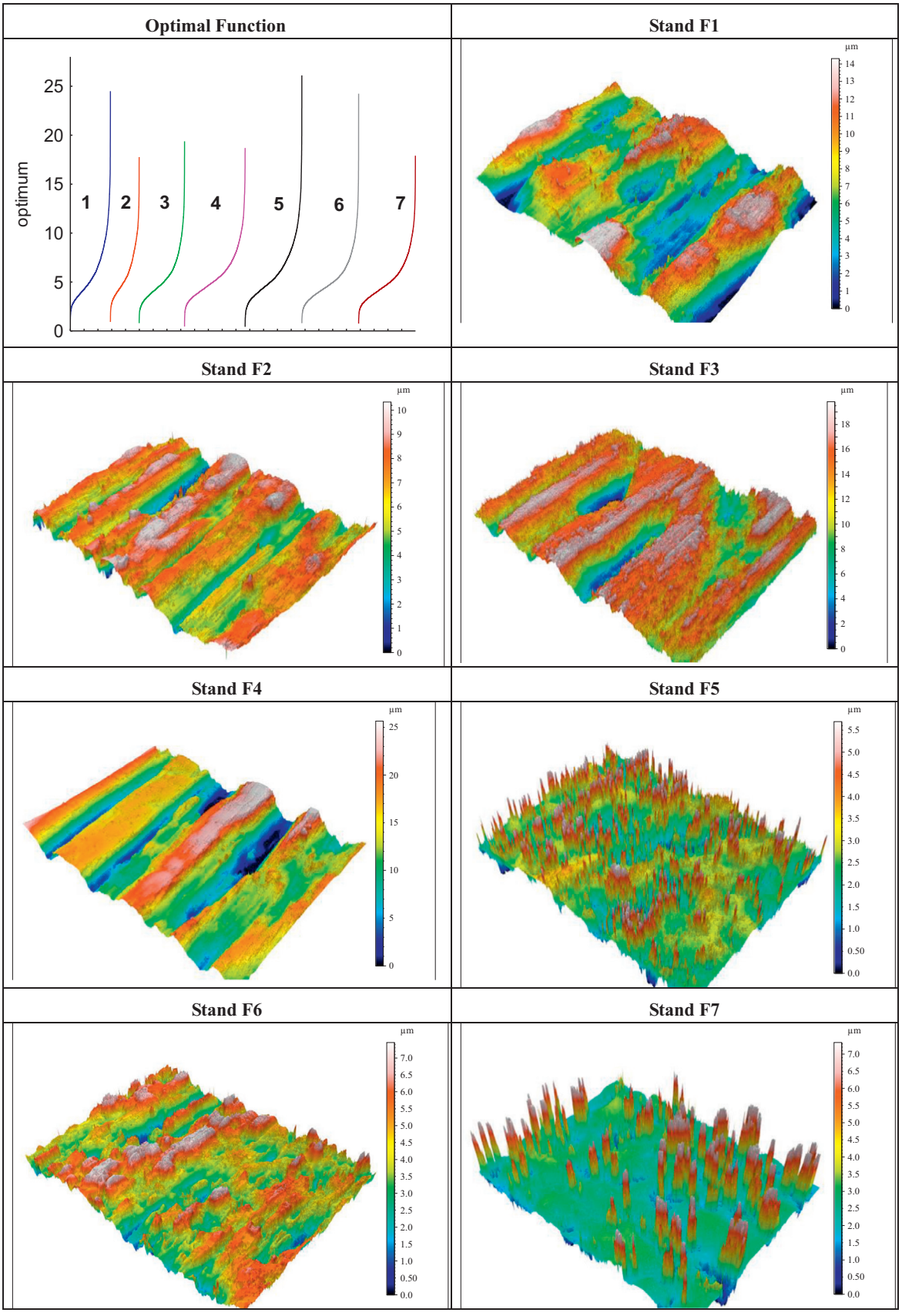

Fig. 14. Evolution of the representative topography for different stands in the hot rolling milling. Small wear (50 km of rolling) and high wear (500 km of rolling). The optimal function $\hat{q}_{i,e,c,k_j}$ is plotted for the seven stands.

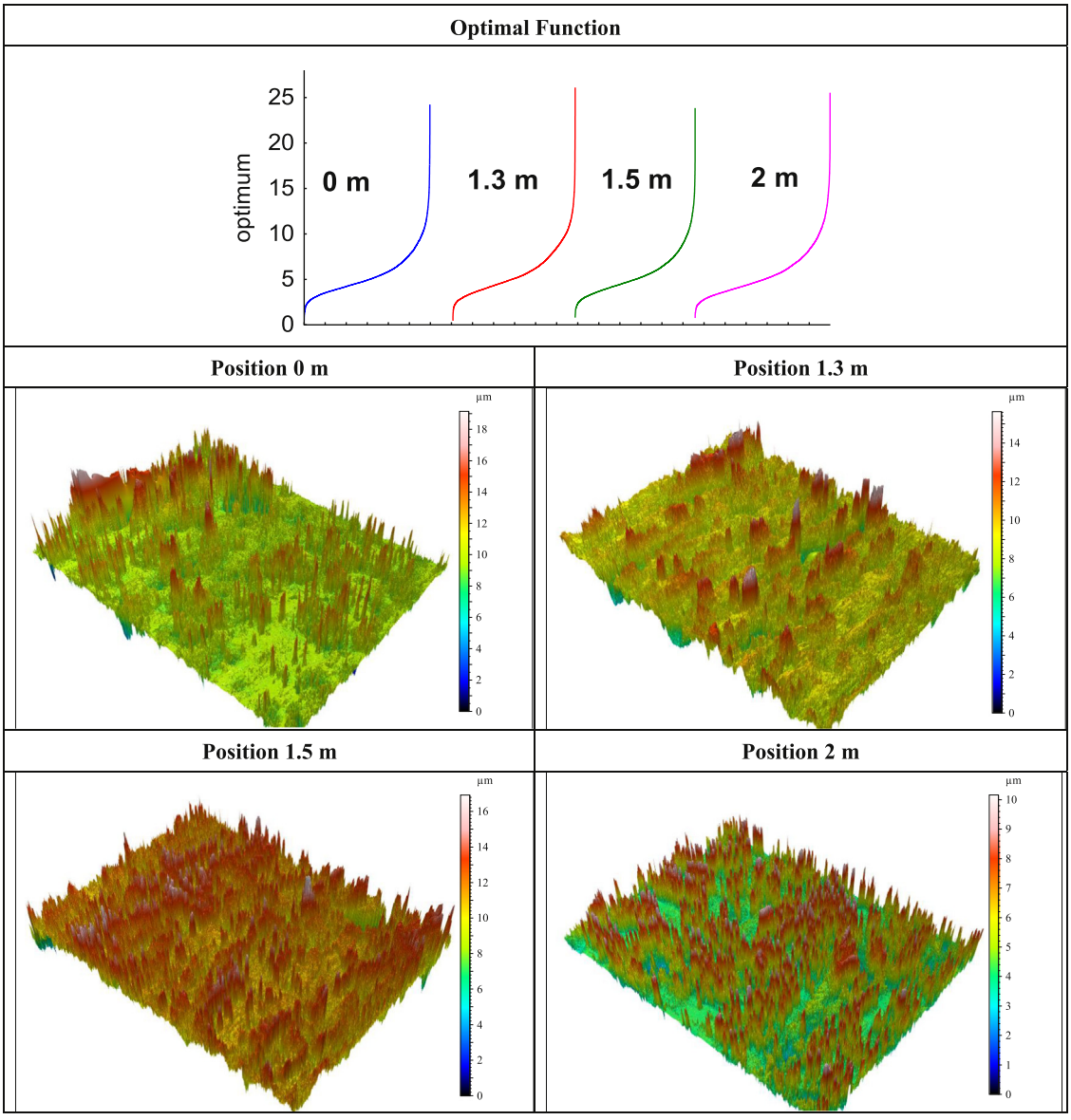

Fig. 15. Evolution of the representative topography along the axis cylinder corresponding center of the coil; 1.3 m coil width: 1.5 m coil width; 2 m coil width (out of the worn area). The optimal function $\hat{q}_{i,e,c,k_j}$ is plotted for the four lateral positions.

surface. Indeed, with increasing wear, the amount of graphite at roll surface will increase, leading to an increase of roll roughness. Based on micrographs of this study, we observed that the corresponding size of graphite precipitates is around 50 µm which could correspond to the size of the dots. The possible oxidation of cementite (Fe_3C carbides) was also confirmed by Chaudansson et al. [17] on ICDP grade at 700 °C.

8. Summary

The method of representative topography allows us to analyze visually the variation of complex topographies of processes. This method allows suppressing anomalous topographical data before using roughness parameters to characterize surface integrities or functionalities. This tool is of major interest to see the map that is the more representative and give a relevant tool to select one topography and to compare with another under different condition. In fact, it could be false to think that we only treat a single map without taking account to another. This original multiscale method allows finding the surface that is experimentally the most probable. Higher will the number of measurements, more precisely will be the representative topographical map. However, this method can be improved in the future by automatically select the anomalous surface and the most representative one. Fundamental aspects will be done by trying to determine the real PDF by when simulated surfaces are used (fractal surfaces).

The method was applied to a practical industrial case: the wear of HSS and ICDP rolls. The observation of replicas made directly on industrial roll workshop after a short and a long rolling campaign allowed us to understand well the degradation of roll surface. Major observations, as the carbides oxidation on unworn areas of the roll, confirmed lab studies performed on equivalent roll materials. The strong interest in this method is to be able to study wear phenomenon of industrial pieces, having big dimensions (difficult to analyze in lab) with a non-destructive protocol. Another major interest is to be able to digest a huge number of data being sure about the reproducibility of results that will help us to find physical explanations to the studied phenomenon.

In a next step, the representativeness of one roll wear will be studied in much more details along three successive campaigns. Finally, the evolution of roughness will be correlated to conventional surface defects size of hot rolling in order to precise some new defect formation mechanisms.

References

[1] Kang YJ, Oh JC, Lee HC, Lee S. Effects of C and Cr additions on the wear resistance and surface roughness of cast HSS cylinders. Metall Mater Trans A 2001;32A:2515–25.

[2] State of the art work rolls for hot rolling flat products. In: Karl Heinz Ziehenberger, Michael Windhager, CONAC 2007—3rd steel industry conference and exposition. Centro Convex, Monterrey, N.L., México; 11th to 14th November 2007.

[3] Sano Y, Hattori T, Haga M. Characteristics of high-carbon high speed steel rolls for hot strip mill. ISIJ Int 1992;32:1194–201.

[4] Bigerelle M, Gautier A, Iost A. Roughness characteristic length scales of micro-machined surfaces: a multi-scale modelling. Sens Actuators, B: Chem 2007;126:126–37.

[5] ISO 11562: 1996, Geometrical product specifications (GPS)—surface texture: profile method—metrological characteristics of phase correct filters. Geneva: International Organization for Standardization; 1996.

[6] ASME B46.1. Surface texture: surface roughness. New York: Waviness, and Lay, American Society of Mechanical Engineers; 1995.

[7] Yuan YB, Vorburger TV, Song JF, Renegar TB. A simplified realization for the Gaussian filter in surface metrology, In: Proceedings of X. international colloquium on surfaces. Aachen: Shaker Verlag GmbH 2000:133–44.

[8] ISO 25178-2:2012 Geometrical product specifications (GPS)—surface texture: areal—Part 2: Terms, definitions and surface texture parameters; 2012.

[9] EUR 15178N. 1993. The development of methods for the characterisation of roughness in three dimensions, Stout, Sullivan, Dong, Mainsah, Luo, Mathia, Zahouani, Commission of the European Communities, EUR 15178EN; 1993.

[10] ISO 12781-1:2011 Geometrical product specifications (GPS)—flatness—Part 1: Vocabulary and parameters of flatness; 2011.

[11] Efron B, Tibshirani RJ. An introduction to the bootstrap. New York: Chapman and Hall; 1985.

[12] Hall P. The bootstrap and the Edgeworth expansion. New York: Springer-Verlag; 1992.

[13] Zhu Q, Zhu HT, Tieu AK, Reid M, Zhang LC. In-situ investigation of oxidation behaviour in high speed steel roll material under dry and humid atmospheres. Corros Sci 2010;52:2707–15.

[14] Zhu Q, Zhu HT, Tieu AK, Kong C. Three dimensional microstructure study of oxide scale formed on a high speed steel by means of SEM, FIB and TEM. Corros Sci 2011;53:3603–11.

[15] Joos O, Boher C, Vergne C, Gaspard C, Nylen T, Rezaï-Aria F. Assessment of oxide scale influence on wear damage of HSM work rolls. Wear 2007;263:198–206.

[16] Ziehenberger KH, Windhager M. State of the art work rolls for hot rolling flat products. In: CONAC 2007—3rd steel industry conference and exposition. Centro Convex, Monterrey, N.L., México; 11th to 14th November 2007.

[17] Chaudansson H, Metivier J, Oxydation des cylindres de laminage, Aperam internal report, RI 92/344; 1992.